JOURNAL OF THERMOPHYSICS AND HEAT TRANSFER
Vol. 21, No. 1, January–March 2007

Technical Notes

TECHNICAL NOTES are short manuscripts describing new developments or important results of a preliminary nature. These Notes should not exceed 2500 words (where a figure or table counts as 200 words). Following informal review by the Editors, they may be published within a few months of the date of receipt. Style requirements are the same as for regular contributions (see inside back cover).

Modeling the Radiation of Participating Media with Coupled Finite Volume Method

Guo-Biao Cai*
Beijing University of Aeronautics and Astronautics, 100083 Beijing, People's Republic of China
Xiao-Ying Zhang†
South China University of Technology, 510640 Guangzhou, People's Republic of China
and
Ding-Qiang Zhu‡
Beijing University of Aeronautics and Astronautics, 100083 Beijing, People's Republic of China

DOI: 10.2514/1.18443

Nomenclature

A_k	=	area of a cell face normal to the kth direction, m^2
a	=	weighting factor in the temperature distribution
b	=	source term in discretization equation, $W/(sr \cdot \mu m)$
D	=	direction cosine integrated over the solid angle
e	=	blackbody emissive power, $W/(m^2 \cdot \mu m)$
f	=	function of gas temperature variation
i	=	radiation intensity, $W/(m^2 \cdot sr \cdot \mu m)$
L_0	=	side length, m
N_p	=	species of particle sizes
N_ω	=	total number of directional angle
$\boldsymbol{n}$	=	unit normal vector
q	=	radiative heat flux, $W \cdot m^{-2}$
R	=	radius, m
r	=	radial distance, m
S_c	=	line intensity
$\boldsymbol{s}$	=	vector defining a direction
T	=	temperature, K
T_0	=	reference temperature, K
V	=	volume, m^3
w	=	weighting factor
X	=	spatial coordinate, m
Z	=	axial length, m
α	=	scattering coefficient, cm^{-1}
β	=	extinction coefficient, cm^{-1}
$\Delta\omega$	=	solid angle interval, sr
δ	=	line spacing in Eq. (10), cm
ε	=	emissivity
θ	=	zenith angle, deg
ϑ	=	scattering albedo
κ	=	absorption coefficient, cm^{-1}
ν	=	wave number, cm^{-1}
ρ	=	density, kg/m^3
σ	=	Stefan–Boltzmann constant
Φ	=	scattering phase function
φ	=	azimuthal angle, deg
Ψ	=	scattering phase function averaged on the incoming and outcoming solid angle
$\nabla\cdot$	=	divergence

Superscripts

$'$	=	direction of incoming radiation
$\bar{}$	=	nondimensionalized parameter

Subscripts

b	=	blackbody
c	=	centerline
e	=	exit
g	=	gas
k	=	spectral band index
n	=	normal to a surface
P, W, E, N, S, R, F	=	control volume index
p	=	particle
w	=	boundary
ν	=	wave number

Received 29 June 2005; revision received 24 August 2006; accepted for publication 26 August 2006.

*Professor, School of Astronautics; cgb@buaa.edu.cn.
†Associate Research Fellow; zhang_xy1119@sina.com.
‡Associate Professor, School of Astronautics; zdq66@buaa.edu.cn.

Introduction

ACCURATE calculation of radiative transfer is of great importance for predicting heat transfer in a combustion system filled with high-temperature gas and particles. Therefore, several methods have been developed to solve the radiative transfer equation in irregular geometry containing emitting, absorbing, and scattering media, such as the finite volume method [1], the discrete ordinates method [2], flux [3], and moment [4] methods.

One of the important issues for radiative heat transfer in a combustion system is the description of the radiative properties of the media gases, which is a mixture of many gases and particles. The models used for defining the radiative properties of combustion gases in radiation calculations can be roughly sorted into three groups [5]: 1) spectral line-by line models, 2) spectral band models, and 3) global models. Among these models, the weighted sum of gray gases model (WSGGM), which replaces the nongray gas behavior by an equivalent finite number of gray gases, has become a highly attractive and practical choice to be used in full modeling of gases and particles. Since Hottel and Sarofim [6] developed this concept in the context of the zonal method, it has been applied to examine the effects of the radiation of spray combustion systems [7] and gas-fired

furnaces [8]. Smith et al. [9], Coppalle and Venisch [10], and others have investigated the weighting factors required for the WSGGM.

The purpose of this work is to theoretically derive the relationship between the weighting factors used in the WSGGM for a mixture of nongray gases and nongray scattering particles, and to develop a new 3-D emitting, absorbing, and scattering media mathematical model and computer code for radiation, based on the coupling of the finite volume method (FVM) and the WSGGM. This work also developed a model that avoids the drawbacks of spectral line and band gas models.

Mathematical Formulation

Applying the weighted sum of gray gases model, the radiative transfer equation (RTE) becomes [11]

$$\frac{\mathrm{d}i_k(\boldsymbol{s})}{\mathrm{d}s} = -(\kappa_{g,k}+\kappa_{p,k}+\alpha_{p,k})i_k(\boldsymbol{s}) + w_{g,k}\kappa_{g,k}i_{b,g} + w_{p,k}\kappa_{p,k}i_{b,p} + \frac{\alpha_{p,k}}{4\pi}\int_{4\pi}\Phi(\boldsymbol{s},\boldsymbol{s}')i_k(\boldsymbol{s}')\,\mathrm{d}\omega \tag{1}$$

where k is an arbitrary spectral band. The corresponding weight factors for gas and particles, as a function of temperature and position, are represented by [11]

$$w_{g,k} = \frac{\int_{\Delta\nu_k} e_{g,b\nu}(T_{g,\nu})\,\mathrm{d}\nu}{e_{g,\nu}(T_g)} \tag{2}$$

The subscript g can be replaced by p for particle. Modest and Zhang [5] have shown that the WSGGM can be used with any solution method, replacing the nongray medium by an equivalent number of gray media with corresponding absorption coefficients.

The FVM has been used to solve the RTE in this paper. In the FVM, space within the interior of the domain of interest is subdivided into discrete nonoverlapping volumes, and a single node is located centrally within each volume. The final discretized equation, which couples the finite volume method with the weighted sum of gray gases model for a general control volume and control angle, can be written as [12]

$$a_P i_{P,k} = a_W i_{W,k} + a_E i_{E,k} + a_S i_{S,k} + a_N i_{N,k} + a_R i_{R,k} + a_F i_{F,k} + b \tag{3}$$

where

$$a_K = \max\lfloor -\Delta A_j D_j, 0\rfloor \tag{4}$$

$$a_P = \sum_{j=1}^{6}\max[\Delta A_j D_j, 0] + \left(\kappa_{g,k} + \sum_{k=1}^{N_P}\kappa_{p,k} + \sigma_{p,k} - \frac{\sigma_{p,k}}{4\pi}\Psi(\boldsymbol{s},\boldsymbol{s})\Delta\omega\right)\Delta V\Delta\omega \tag{5}$$

$$b = \left(w_{g,k}\kappa_{g,k}i_{b,g} + w_{p,k}\kappa_{p,k}i_{b,p} + \frac{\sigma_{p,k}}{4\pi}\sum_{\boldsymbol{s}'=1,\boldsymbol{s}'\neq\boldsymbol{s}}^{N_\omega} i(\boldsymbol{s}')\Psi(\boldsymbol{s},\boldsymbol{s}')\Delta\omega'\right)\Delta V\Delta\omega \tag{6}$$

$$\Delta\omega = \int_{\phi-\Delta\phi/2}^{\phi+\Delta\phi/2}\int_{\theta-\theta/2}^{\theta+\theta/2}\sin\theta\,\mathrm{d}\theta\,\mathrm{d}\phi \tag{7}$$

$$\Psi(\boldsymbol{s},\boldsymbol{s}') = \frac{\int_{\Delta\omega}\int_{\Delta\omega'}\Phi(\boldsymbol{s},\boldsymbol{s}')\,\mathrm{d}\omega\,\mathrm{d}\omega'}{\Delta\omega\Delta\omega'} \tag{8}$$

The boundary condition at a gray diffuse wall with a prescribed temperature can be written as

$$i_{w,\nu}(\boldsymbol{s}) = \varepsilon_w i_{bw,\nu} + \frac{(1-\varepsilon_w)}{\pi}\int_{\boldsymbol{s}'\cdot\boldsymbol{n}<0} i_{w,\nu}(\boldsymbol{s}')\boldsymbol{s}'\cdot\boldsymbol{n}_w\,\mathrm{d}\omega' \tag{9}$$

The radiative heat flux on a boundary surface can be calculated by integrating radiative intensity

$$q = \int_{\nu=0}^{\infty}\left(\int_{\varphi=0}^{\pi}\int_{\theta=0}^{2\pi} i'_\nu\sin\theta\,\mathrm{d}\theta\,\mathrm{d}\varphi\right)\mathrm{d}\nu \tag{10}$$

The solution of Eqs. (3–10) is based on evaluating spectral optical properties of gases. This work is done for a mixture of CO_2 and H_2O and particles. The absorption coefficients for CO_2 and H_2O used in the WSGGM are calculated by the narrrow-band model [11], which is based on spectral calculations. The Elsasser narrow-band model is used in conjunction with the correlation parameters in Edwards' wide-band model, which is given as follows [11]:

$$\kappa_\nu = \frac{S_c}{\delta}\frac{\sinh(\pi\beta/2)}{\cosh(\pi\beta/2) - \cos[2\pi(\nu-\nu_c)/\delta]} \tag{11}$$

The spectral optical properties of particles could be computed by Mie theory, which can be found in [11].

Test Cases

One test case is defined for the three-dimensional rectangular enclosure. The enclosure is filled with gray, absorbing, emitting, and scattering media with gray and diffuse walls. Results are given in nondimensional quantities such as: $\bar{i} = i/4\sigma T_0^4$, $\bar{q} = q/\sigma T_0^4$, where T_0 is the reference temperature. The optical coefficients are nondimensionalized as: $\bar{\kappa} = \kappa L_0$, $\bar{\alpha} = \alpha L_0$. The scattering phase functions used in the anisotropic scattering problems are those given by Kim and Lee [13] and shown in Fig. 1, where F1 and F2 are forward scattering phase functions whereas B1 and B2 are backward scattering. Another case is a cubic enclosure with side length L_0, which is filled with an isothermal medium at temperature T_0, and absorbs, emits, and scatters anisotropically. The walls of the enclosure are cold at 0 K and black.

The last case is taken from Liu's paper [14]. Those results, obtained by the statistical narrow-band (SNB) model, are considered as the most accurate and are used here as the benchmark. There are three test cases in [14]. To verify the mathematical model and computer code developed herein, a comparison was performed against case 3. In that case, the medium composition is a uniform gas mixture of 10% CO_2, 20% H_2O, and 70% N_2 on a molar basis. The temperature field of the gas is nonuniform and symmetric about the centerline of the enclosure. The temperature can be obtained from the expression $T = (T_c - T_e)f(r/R) + T_e$, where T_c is the gas temperature along the centerline of the enclosure and T_e is the exit temperature. The centerline temperature T_c increases linearly from 400 K at the inlet $Z = 0$ to a maximum value of 1800 K at $Z =$ 0.375 m and then decreases linearly to 800 K at the exit $Z = 4$ m.

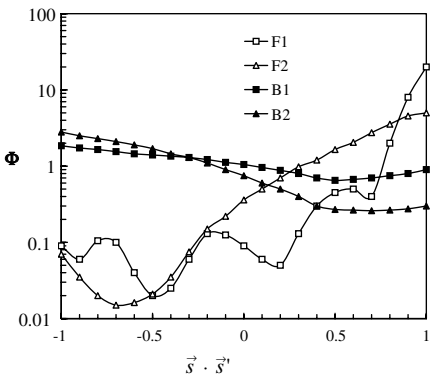

Fig. 1 Scattering phase functions formed by Legendre series.

Inside the enclosure, a circular region or a cylinder around the centerline can be imagined, where the radius of the cylinder is $R = 1$ m. The variation of gas temperature within the circular region of the enclosure's cross section is given by the equation $f(r/R) = 1 - 3(r/R)^2 + 2(r/R)^3$, where r is the distance from the centerline of the enclosure. The gas temperatures outside the circular region, i.e., between the cylinder with radius $R = 1$ m and the walls of rectangular enclosure, were defined as uniform and equal to the value of the exit temperature $T_e = 800$ K.

Numerical Prediction

Figure 2 shows the radiative heat flux $\bar{q}$ along a line which is from the origin through the point $(L_0, L_0/2, L_0)$, assuming isotropic scattering. The extinction coefficient β and the scattering albedo $\vartheta = \alpha/\beta$ are 1 and 0.5, respectively. The results from the FVM with the WSGGM are compared with those of the Monte Carlo method without scattering. The results from the Monte Carlo method without scattering are higher than those of the FVM with the WSGGM. The reason is that more energy is dissipated within the media before reaching the boundary when particle scattering is considered in the FVM. This is in accordance with the results in [15], in which the parameter $i(\vartheta)/i(0)$ of a uniform planar medium decreases from 1 to 0 when ϑ increases from 0 to 1.

Figure 3 shows the incident radiation along the centerline of the enclosure $(X, L_0/2, L_0/2)$ for different scattering phase functions and two wall emissivities, 1 and 0.5. The walls are cold at 0 K and reflect radiation diffusely. The extinction coefficient β and the scattering albedo $\vartheta = \alpha/\beta$ are 2 and 0.5, respectively. Note that the incident radiation shows strong dependence on the scattering phase function. The maximum difference occurs at the location of the maximum incident radiation near the center of the enclosure. The forward scattering medium gives lower incident radiation than the isotropically scattering medium, which again gives lower incident radiation than the backward scattering medium. The backward scattering medium tends to block the transfer of radiative energy to the walls and absorbs more energy. One can also note that the incident radiation increases and becomes spatially flatter as the emissivities decrease in Fig. 3. The differences among the solutions with different scattering phase functions also decrease as the wall emissivities decrease, because the diffuse reflection at the walls tends to compensate for the effect of anisotropic scattering.

Figures 4 and 5 show the effect of anisotropic scattering on the radiative heat flux and incident radiation as the optical thickness varies. The extinction coefficient β is assumed to be 1, 2, and 10, whereas the scattering albedo ϑ is fixed as 0.5. Figure 4 shows the radiative heat flux $\bar{q}$ along the line $(X, L_0/2, L_0)$. The effect of anisotropic scattering is negligible when β is equal to 1, whereas some variation due to the different scattering phase functions is shown when β is equal to 2. The effect of anisotropic scattering causes significant variation in the radiative heat flux when β is equal to 10. Figure 5 shows the incident radiation along the line $(X, L_0/2, L_0/2)$. Note that anisotropic scattering affects the incident radiation at lower optical thickness more than for the radiative heat flux in Fig. 4. This is because the scattered radiation contributes to an increase in the incident radiation, whereas the scattering may increase or decrease the radiative heat flux according to the propagation direction after scattering.

For test case 3, the predictions are shown in Figs. 6 and 7. Figure 6 shows the radiative heat source along centerline $(L_0/2, L_0/2, Z)$

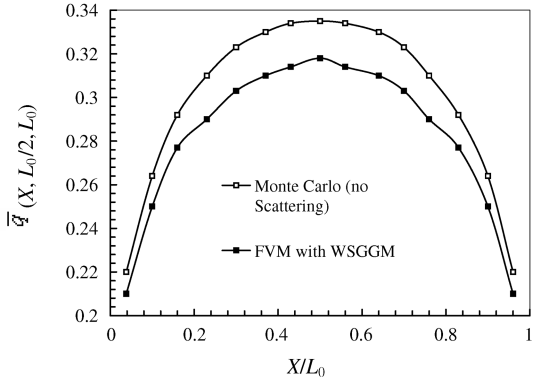

Fig. 2 Nondimensional radiative heat flux for test case 1.

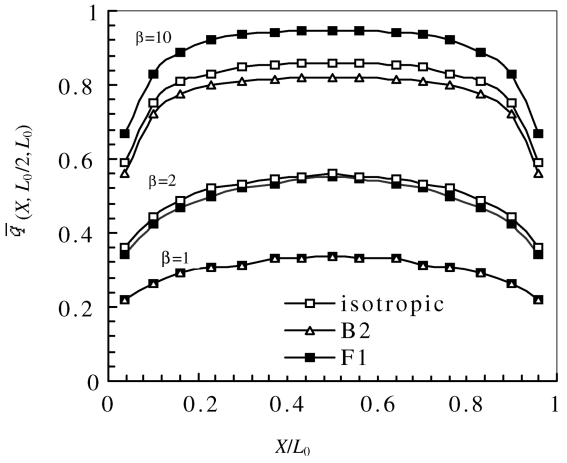

Fig. 4 Effect of anisotropic scattering on radiative heat flux for different optical thicknesses.

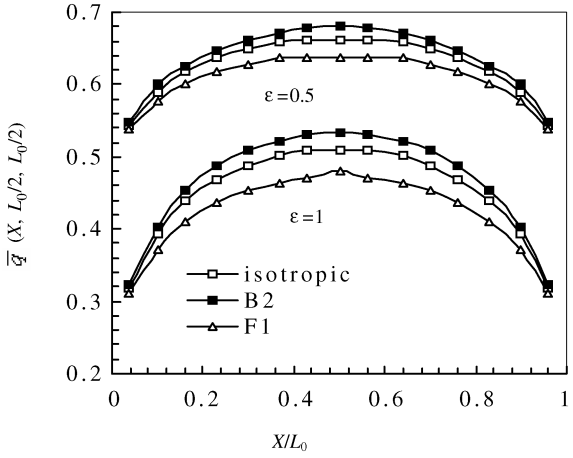

Fig. 3 Effect of anisotropic scattering and wall emissivity on incident radiation, test case 2.

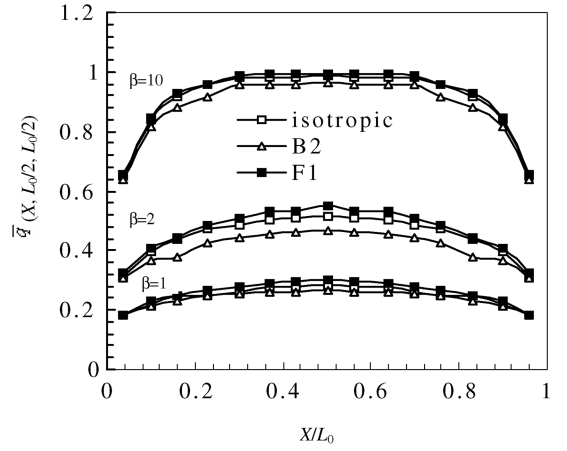

Fig. 5 Effect of anisotropic scattering on incident radiation for different optical thicknesses.

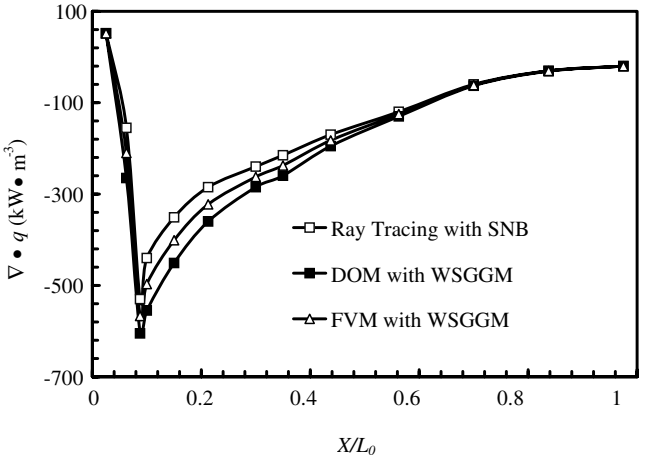

Fig. 6 Predictions of radiative heat source for test case 3.

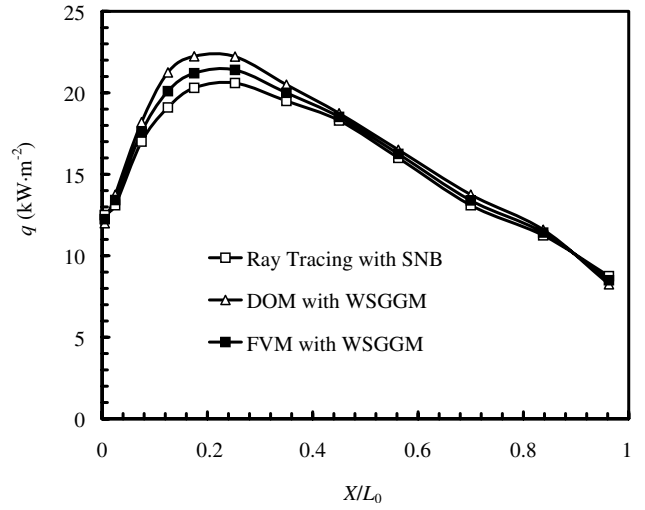

Fig. 7 Predictions of radiative heat flux for test case 3.

predicted by the FVM with the WSGGM as well as the results calculated by ray tracing with the SNB [14] and the discrete ordinates method (DOM) with the WSGGM [16]. Figure 7 gives the incident heat flux along $(L_0, L_0/2, Z)$ predicted by the FVM with the WSGGM as well as the results calculated by ray tracing with the SNB [14] model and the DOM with the WSGGM [16].

It can be seen from Fig. 6 that the prediction of the radiative heat source obtained by the FVM with the WSGGM are very close to, or almost identical to, the results obtained from the DOM with WSGGM [14]. This could be expected because the DOM and the FVM are very similar methods. Figure 7 shows that the predictions of heat flux calculated by the FVM with the WSGGM and by the DOM with the WSGGM [14] are close to each other.

Conclusions

A new mathematical model and computer code have been developed which couple the FVM and the WSGGM for radiative transfer in emitting, absorbing, and scattering media. The physical and mathematical concepts of the model were roughly presented. Two cases were presented for 3-D rectangular and cylindrical enclosures. The predictions were compared to the results found in the literature, which showed good agreement with each other.

Radiative heat flux from a mathematical method without scattering is slightly higher than that from the method with scattering. The forward scattering media give lower incident radiation than the isotropic scattering media, which again give lower incident radiation than the backward scattering media. As the wall emissivities decrease, the incident radiation increases and becomes spatially flatter, and the differences among the solutions with different scattering phase functions decrease also.

The WSGGM can avoid a large quantity of work needed to compute spectral lines and bands by an equivalent finite number of gray gases. The FVM is now widely used to solve the radiation transfer equation in emitting, absorbing, and scattering media. By coupling the WSGGM and the FVM, a new convenient method for predicting radiative transfer in combustion systems has been established.

References

[1] Raithby, G. D., and Chui, E. H., "Finite-Volume Method for Predicting a Radiant Heat Transfer in Enclosures with Participating Media," *Journal of Heat Transfer*, Vol. 112, No. 2, 1990, pp. 415–423.

[2] Fiveland, W. A., "Discrete-Ordinates Solutions of the Radiative Transport Equation for Rectangular Enclosures," *Journal of Heat Transfer*, Vol. 106, No. 4, 1984, pp. 699–706.

[3] Selcuk, N., "Evaluation of Multi-Dimensional Flux Models for Radiative Transfer in Combustors," *International Journal of Heat and Technology*, Vol. 13, No. 2, 1995, pp. 73–90.

[4] Viskanta, R., and Menguc, M. P., "Radiation Heat Transfer in Combustion Systems," *Progress in Energy and Combustion Science*, Vol. 13, No. 2, 1987, pp. 97–160.

[5] Modest, M. F., and Zhang, H., "The Full-Spectrum Correlated-k Distribution and Its Relationship to the Weighted-Sum-of Gray-Gas Method," *Proceedings of the ASME Heat Transfer Division*, Vol. 366, American Society of Mechanical Engineers, New York, 2000, pp. 75–84.

[6] Hottel, H. C., and Sarofim, A. F., *Radiative Transfer*, McGraw–Hill, New York, 1967, Chap. 13.

[7] Choi, C. E., and Baek, S. W., "Numerical Analysis of a Spray Combustion with Non-Gray Radiation Using Weighted Sum Gray Gases Model," *Combustion Science and Technology*, Vol. 115, No. 4, 1996, pp. 297–315.

[8] Liu, F., Becker, H. A., and Bindar, Y., "A Comprehensive Study of Radiative Heat Transfer Modelling in Gas-Fired Furnaces Using the Simple Gray Gas and the Weighted-Sum-of-Gray-Gases Models," *International Journal of Heat and Mass Transfer*, Vol. 41, No. 21, 1998, pp. 3357–3371.

[9] Smith, T. F., Shen, Z. F., and Friedman, J. N., "Evaluation of Coefficients for the Weighted Sum of Gray Gases Model," *Journal of Heat Transfer*, Vol. 104, No. 4, 1982, pp. 602–608.

[10] Coppalle, A., and Venisch, P., "The Total Emissivities of High Temperature Flames," *Combustion and Flame*, Vol. 49, No. 1, 1983, pp. 101–108.

[11] Siegel, R., and Howell, J. R., *Thermal Radiation Heat Transfer*, 3rd ed., Hemisphere, Washington, D.C., 1992, Chap. 13.

[12] Fan, S. W., Zhang, X. Y., Zhu, D. Q., and Cai, G. B., "Calculation of the Infrared Characteristics of the Solid Rocket Plume with FVM Method," *Journal of Astronautics*, Vol. 26, No. 6, 2005, pp. 793–797.

[13] Kim, T. K., and Lee, H. S., "Effect of Anisotropic Scattering on Radiative Heat Transfer in Two-Dimensional Rectangular Enclosures," *International Journal of Heat and Mass Transfer*, Vol. 31, No. 8, 1988, pp. 1711–1721.

[14] Liu, F., "Numerical Solutions of Three-Dimensional Non-Gray Gas Radiative Transfer Using the Statistical Narrow-Band Model," *Journal of Heat Transfer*, Vol. 121, No. 2, 1999, pp. 200–203.

[15] Freeman, G. N., Ludwig, B., Malkmus, W., and Reed, R., "Development and Validation of Standardized Infrared Radiation Model (SIRRM), Gas/Particle Radiation Transfer Model," U.S. Air Force Rocket Propulsion Laboratory Rept. AD-A076199, Edwards AFB, CA, 1979.

[16] Coelho, P. J., "Numerical Simulation of Radiative Heat Transfer from Non-Gray Gases in Three-Dimensional Enclosures," *Journal of Quantitative Spectroscopy and Radiative Transfer*, Vol. 74, No. 3, 2002, pp. 307–328.